

1 Non-parabolicity and band gap re-normalisation in Si doped ZnO

2 R. E. Treharne* and L. J. Phillips, K. Durose

3 *Stephenson Institute for Renewable Energy, University of Liverpool, UK*

4 A. Weerakkody, I. Z. Mitrovic, S. Hall

5 *Department of Electrical Eng. and Electronics, University of Liverpool, UK*

6 (Dated: September 18, 2013)

7 Abstract

8 A combinatorial methodology, developed for the rapid optimisation of sputtered transparent
9 conducting oxides, is applied to Si doped ZnO. A wide range of compositions are explored over a
10 single sample to determine an optimum composition, with respect to the minimisation of resistivity,
11 of $x = 0.65\%$ wt. SiO_2 . A fundamental investigation of the conduction band non-parabolicity yields
12 values of $m_{e0} = 0.35m_0$ and $C = 0.3 \text{ eV}^{-1}$ for the conduction band minimum effective mass and
13 the non-parabolicity factor respectively. Further analysis of extracted band gap values with respect
14 to dopant concentration provides an estimate of the magnitude of re-normalization effects. Finally,
15 a model is proposed to describe the carrier transport behaviour for a degenerate polycrystalline
16 semiconductor by accounting for the tunnelling of carriers through grain boundaries.

17 PACS numbers: 78.20.Jq, 88.66.sq, 81.15.-z

18 Keywords: zinc oxide; magnetron sputtering; thin-film; doping; non-parabolicity, band gap normalisation

19 INTRODUCTION

20 Polycrystalline ZnO films have received significant attention in recent years. They can
21 be degenerately doped, typically by incorporating group III (e.g. Al, Ga or In [?]) or group
22 VII (e.g. F [? ?], Cl [?]) elements to achieve resistivities of the order $10^{-4} \Omega\text{.cm}$, while
23 maintaining a high optical transparency ($> 80\%$). Such ZnO based transparent conducting
24 oxide (TCO) films, most notably Al doped ZnO (AZO), are now used extensively within thin-
25 film photovoltaic technologies (namely CIGS, CZTS and CdTe) and have widely replaced the
26 use of indium based TCOs. A wide range of deposition techniques has been demonstrated
27 for ZnO films including atomic layer deposition (ALD) [?], metal-organic chemical vapour
28 deposition (MOCVD) [?], pulsed laser deposition (PLD) [?] and magnetron sputtering [?
29 ? ?].

30 The key property of a TCO is its resistivity, which in the context of thin-film PV,
31 should be as low as possible. Film transmittance will generally remain high over the visible
32 wavelength range for a wide range of resistivities, except in the case of exceptionally high
33 free carrier concentrations (i.e. $> 10^{21} \text{ cm}^{-3}$), and so is of secondary concern experimentally.
34 The most common approach to minimising a TCO's resistivity is to generate large sample
35 sets over which a single experimental parameter (e.g. pressure, temperature, composition)
36 is varied incrementally. Such investigations are time consuming and the experimental con-
37 sistency from sample to sample can be poor due to uncontrollable drifts in other associated
38 deposition parameters. Furthermore, even for large sample sets the relationship determined
39 between the resultant film properties and the deposition conditions can often be ambiguous.
40 This is particularly true for resistivity which is highly sensitive and can vary on the scale of
41 several orders of magnitude for a very narrow range of composition.

42 In this work, a combinatorial methodology is developed for the study of TCO materials
43 and demonstrated in the case Si doped ZnO (SZO). The approach eliminates the need
44 for large sample sets and generates results that are highly consistent and reliable. We
45 demonstrate how the methodology can be used to investigate fundamental properties of the
46 material, namely conduction band non-parabolicity and band gap re-normalization, as well
47 as more empirical relationships such as the compositional dependence of electrical properties.
48 Furthermore, the consideration of a grain boundary limited scattering mechanism to describe
49 the observed transport behaviour in SZO leads to the proposal of an extension to the current

theory to apply in the case of degenerately doped polycrystalline films.

EXPERIMENTAL METHODS

Films were deposited via RF magnetron sputtering using an AJA Phase II-J Orion system. The system was configured in a ‘sputter-up’ geometry with the substrate being suspended above two separate ceramic targets of ZnO and SiO₂ arranged off-centre and tilted at 5° towards the centre of the substrate. Soda-lime glass substrates (OptiWhiteTM, NSG Pilkington) of size 100 × 100 × 4 mm³ were cleaned by scrubbing with a nylon brush and a series of de-ionized water and isopropanol alcohol rinses followed by blow drying with a nitrogen gas jet. During deposition the ZnO and SiO₂ targets were sputtered simultaneously using powers of 150 W and 50 W respectively. A growth pressure of 2.7 × 10⁻³ mbar Ar was used during deposition. The substrate temperature was maintained at 350 ± 5°C during growth and the substrate was kept static with respect to the magnetrons (i.e the substrate was not rotated). Deliberate gradients of both thickness and composition were therefore incorporated across the resultant film to generate a ‘combinatorial’ sample. A second film of pure SiO₂ was deposited under identical conditions (but without ZnO) to generate a reference film for estimating the % wt. profile of SiO₂ in the co-sputtered combinatorial sample.

A Shimadzu UV-Vis-IR 3700 spectrophotometer with mapping capability was used to measure the transmittance of the co-sputtered film over the range 250 - 2500 nm. 289 spectra were taken in total at 5 mm increments over the full sample surface. At each of these 289 points the sheet resistance was also measured using a CMT-SR2000 4-point probe mapping system. Following transmittance and sheet resistance measurements the sample was cut into one hundred 10 × 10 mm² pieces. A selection of these pieces, 10 in total, were further scribed into four 5 × 5 mm² sections and Hall measurement were performed on each of these sections. Hall measurements were performed with custom built equipment, provided by Semimetrix Ltd., using a field strength of 0.8 T. Ellipsometry was performed on the same sections using a Woollam M2000-UI system. Ellipsometry was also used to map the thickness profile of the pure SiO₂ reference film.

77 RESULTS

78 Fitting of optical spectra

79 Figure 1 shows a typical transmittance spectra taken from a single point on the combi-
80 natorial ZnO:Si sample and the corresponding fit achieved using a theoretical model of the
81 material's dielectric permittivity $\varepsilon(\omega)$. Full details of this model are given in [?]. The key
82 components of the model include: 1) a Lorentzian oscillator to account for the behaviour of
83 the system's bound electrons and to provide a smoothly varying dielectric background over
84 the range of interest (250 – 2500 nm), 2) an extended Drude model [?], to characterise the
85 system's free electron response, and 3) an inter-band transition model to account for the
86 steep increase in the material's absorption coefficient in the vicinity of its direct band gap
87 (3.3 – 3.4 eV). The two key parameters extractable from the dielectric model are the film's
88 thickness, d , and plasma frequency, ω_p , which is related directly to the carrier concentration
89 according to

$$\omega_p = \sqrt{\frac{n_e e^2}{m_e \varepsilon_\infty \varepsilon_0}} \quad (1)$$

90 where m_e is the effective electrons (expressed in units of the free electron mass, m_0), ε_∞ is
91 the material's high frequency relativity permittivity (~ 8.3 for single crystal ZnO [?]) and
92 ε_0 is the permittivity of free space. Note that as ε_∞ is not known for the specific sample, the
93 combined product $\varepsilon^{1/1}\omega_p$ is extracted as a single parameter from the model and here-in the
94 term 'plasma frequency' refers to this product. The optical dispersion for the material, i.e.
95 refractive index n and extinction coefficient κ , is also extracted from the fitting procedure
96 and the spectra are shown in the inset of figure 1.

97 Fitting was achieved by using a Nelder-Mead downhill simplex algorithm [?], imple-
98 mented via python script, to minimize the quantity

$$\chi^2 = \sum_i^N \sqrt{\frac{y_i - O_i}{N^2}} \quad (2)$$

99 where N is the total number of data points in the spectra, O_i the observed transmittance at
100 each wavelength over the range of interest, and y_i the theoretical transmittance calculated
101 using the transfer matrix method [?] for a single thin-film on a finite, transparent substrate.
102 The fitting algorithm was iterated until the relative fractional change in consecutive χ^2
103 values was less than 1×10^{-6} . The fitting of all 289 transmittance spectra taken over the

combinatorial sample was fully automated, the only user input required being an initial estimate of film thickness at the point of the first spectrum. This automation ensured that the fitting of consecutive spectra was highly consistent. For all spectra, χ^2 values of < 2 were achieved indicating that all fits were as successful as that shown in figure 1.

It was not possible to extract values for the true optical band-gap E_G from the inter-band transition component of the model which relied on a simple $\alpha \propto (E - E_G)^{1/2}$ dependence to describe the behaviour in the vicinity of the band edge. All values of E_G were typically $\sim 0.2 - 0.4$ eV lower than expected, even once non-parabolicity and re-normalisation effects had been accounted for, see sections and). This is due to the presence of a population of impurity states located in energy just below the bottom of the conduction band. The presence of these states generates a broadening, commonly referred to as an ‘Urbach tail’ [?], in the onset of the absorption coefficient. It is very difficult to determine the extent of this broadening by fitting the dielectric model to a single transmittance spectra. The use of variable angle ellipsometry permitted a more reliable extraction of the band gap values due to the requirement that the fitting procedure satisfied multiple spectra simultaneously.

For each point over the combinatorial sample ellipsometric spectra were taken at angles of 65° and 70° with respect to a plane normal to the sample surface. The spectra were fitted using a parameterized semi-conductor (PSEMI-M0) model [?] over the range $350 - 1000$ nm. Figure 2b shows a typical fit achieved by the model and the inset shows the difference in the α^2 versus E behaviour extracted from transmittance and ellipsometry data respectively. This disparity between band gaps extracted from the two techniques is in good agreement with that reported by Srikant [?] in ZnO.

Conduction band non-parabolicity

For highly doped metal-oxides it has been shown that the conduction band, E_c , is ‘non-parabolic’ and that the origin of this non-parabolicity may be attributed to a carrier dependent effective mass, $m_e(n_e)$. The functional form of this dependence, first suggested by Pisarkiewicz *et. al* [?], is given by

$$m_e(n_e) = m_{e0} \sqrt{1 + \frac{2C\hbar^2 k}{m_{e0}}} \quad (3)$$

where m_{e0} is the value of the effective mass at the conduction band minimum and C is the non-parabolicity factor, expressed in eV^{-1} . The carrier wave-number can be expressed in terms of the carrier concentration according to $k = (3\pi^2 n_e)^{1/3}$. By re-examining equation 1 it is clear that the relationship between ω_p^2 and n_e becomes non-linear if the effective mass is not a constant. Figure 3 shows a plot of ω_p , extracted from the spectrophotometry measurements, versus the carrier concentration, n_e^H , determined via Hall measurements, for the sample subset cut from the original combinatorial sample. A similar χ^2 minimization procedure to that described in section , in which the fitting parameters were m_{e0} and C , was applied to the data set using

$$\chi^2 = \sum_{i=1}^n \frac{(n_{e_i}^S - n_{e_i}^H)^2}{n^2} \quad (4)$$

where the superscript S corresponds to carrier concentrations calculated, using a carrier dependent effective mass $m_e(n_e)$ (equations (1) and 3), from the spectroscopically determined plasma frequencies. The superscript H denotes values of n_e determined directly from Hall measurements. To determine the uncertainty associated with the fitted m_{e0} and C values, Monte-Carlo style error treatment [?] was implemented within which the χ^2 minimization procedure was performed 1000 times. The inset plot in figure 3 shows the mean $m_e(n_e)$ relationship (solid line) and the corresponding spread (yellow line). An average extracted value of $m_{e0} = 0.35 \pm 0.02 m_0$ is higher than previous published values of $0.24 - 0.28 m_0$ for the effective mass in undoped ZnO. An average extracted value of $C = 0.30 \pm 0.01 \text{ eV}$ agrees very well with previously reported values of $\sim 0.29 \text{ eV}^{-1}$ [?] for Al doped ZnO films.

Band-gap renormalization

The optical band gap of a degenerately doped metal-oxide system increases as a function of carrier concentration (Burstein-Moss shift [?]) according to

$$E_G = E_{G0} + \frac{\hbar^2 (3\pi^2 n_e)^{2/3}}{2m_{JDOS}} \quad (5)$$

where E_{G0} is the band-gap at the conduction band minimum and the joint density of states effective mass, m_{JDOS} is given as

$$\frac{1}{m_{JDOS}} = \frac{1}{m_h} + \frac{1}{m_e(n_e)} \quad (6)$$

155 A constant hole effective mass value of $m_h = 0.7m_0$ [? ?] is assumed throughout this work.
 156 Note that the non-parabolicity of the conduction band is accounted for when estimating the
 157 band gap by the use of the carrier dependent effective mass $m_e(n_e)$ determined in section .
 158 The data points in figure 4 show the band-gap values, determined from ellipsometry, plotted
 159 against the Hall carrier concentrations. The points lie some distance from the relationship
 160 predicted by equation 5. The apparent reduction in the real band-gap values is due the
 161 re-normalization effects of many body electron-electron, electron-ion and electron-hole in-
 162 teractions. Lu *et. al* [?] have shown that the total energy shift due to re-normalization
 163 can be estimated by parameterising the detailed model described by Jain *et. al* [? ?]
 164 according to

$$E_R = An_e^{1/3} + Bn_e^{1/4} + Cn_e^{1/2} \quad (7)$$

165 where E_R is negative with respect to E_G . The $n_e^{1/3}$, $n_e^{1/4}$ and $n_e^{1/2}$ dependencies correspond to
 166 the exchange energy of free electrons, their correlation energy and the electron-ion interaction
 167 energy respectively. The coefficients A , B , and C , quantify the strength of each of these
 168 three dependencies. The coefficient values and a value for E_{G0} , was extracted using the
 169 established minimisation procedure. Table I shows the extracted values and comparative
 170 values for n-type ZnO thin-films. The strength of the $n_e^{1/3}$ dependence is roughly three times
 171 than that reported for Al doped ZnO but vales for the other two coefficients are consistent
 172 [?].

173 MAPPING OF COMPOSITIONAL DEPENDENCE

174 Film thickness profiles were determined for the combinatorial ZnO:Si and SiO₂ samples.
 175 The % wt. SiO₂ content at each point over the combinatorial sample was estimated according
 176 to

$$x = \frac{\Gamma_B d_B}{\Gamma_A d_A + \Gamma_B d_B} \times 100\% \quad (8)$$

177 where Γ_A and Γ_B are the bulk densities of ZnO and SiO₂ respectively and d_A and d_B are
 178 the corresponding thicknesses, d , of the ZnO and SiO₂ films. The carrier concentration
 179 profile for the combinatorial sample was calculated from extracted $\varepsilon_\infty^{1/2}\omega_p$ values according
 180 to equation 1 and using the non-parabolic effective mass relationship, $m_e(n_e)$, determined

181 in section . The corresponding mobility profile was calculated using

$$\mu_e = \frac{1}{n_e^S R_S d e} \quad (9)$$

182 where R_S are the sheet resistance values obtained directly from 4 point probe measurements.
 183 Figure 5 shows the three dimensional contour profiles of n_e and μ_e across the surface of the
 184 combinatorial sample. In both cases, a maximal ridge, corresponding to $n_e \sim 4.5 \times 10^{20}$
 185 cm^{-3} and $\mu_e \sim 16 \text{ cm}^2\text{V}^{-1}\text{s}^{-1}$, runs diagonally across the sample. By superimposing the
 186 contour distribution of ρ . (dotted black contour lines), a very strong correlation between
 187 carrier concentration and composition becomes apparent, the maximum n_e and μ_e values
 188 corresponding to a value of $x = 0.65\%$ and a minimum resistivity of $8.6 \times 10^{-4} \Omega.\text{cm}$.

189 By plotting the distributions of n_e and μ_e with respect to x the compositional dependence
 190 can be observed directly as shown in figure 6. Here the strength of the combinatorial analysis
 191 is fully appreciated by its ability to generate continuous, non-ambiguous distributions of
 192 the material's electrical behaviour and shows that it is highly sensitive to the composition
 193 - the resistivity spanning over three orders of magnitude within the compositional range
 194 $x = 0 - 0.65\%$. Furthermore, the uncertainty in the optimum value of x , that minimises
 195 the resistivity, is significantly reduced when compared to the multi-sample analyses that are
 196 commonly reported.

197 The solid straight line in the n_e vs x plot indicates the relationship predicted for a 100%
 198 doping efficiency, i.e. where every Si atom incorporated into film substitutionally replaces
 199 a Zn atom and contributes two free electrons to the system. For low values of x , i.e. in
 200 the range $x = 0 - 0.5\%$, this relationship is adhered to. However as x increases further the
 201 doping efficiency decreases rapidly and the carrier concentration is limited to $3 - 4 \times 10^{19} \text{ cm}^{-3}$
 202 for compositions up to 10% wt. SiO_2 . After the optimum value of x is reached, the mobility
 203 drops off steeply and approaches a value of zero for values of x beyond 6%. This suggests
 204 that as x is increased beyond the optimum composition, Si is incorporated interstitially
 205 rather than substitutionally or forming segregated Si-) phases at the grain boundaries, thus
 206 acting to increase free carrier scattering and so reducing mobility.

208 The behaviour of carrier mobility can be described further by considering its direct re-
 209 lationship with the carrier concentration. Figure 7 shows that by plotting μ_e versus n_e for
 210 all data points in the range $0 < x < 0.65\%$ a well defined, unambiguous relationship is
 211 determined. The red data points correspond to compositions $x < 0.65\%$. Within this distri-
 212 bution, and for carrier concentrations below $2.5 \times 10 \text{ cm}^{-3}$ the mobility of the free carriers
 213 can be described in terms of the grain barrier limited transport model proposed by Seto *et.al*
 214 [?]. The model assumes that at the grain boundaries a population of filled and charged
 215 trap states exists within the band gap. This causes the conduction band to bend upwards
 216 at each grain boundary forming a barrier to charge transport. The inter-grain mobility, μ_B
 217 of free carriers is therefore limited by thermal processes according to

$$\mu_{ig} = \mu_0 \exp\left(-\frac{\Phi_B}{k_B T}\right) \quad (10)$$

218 where Φ_B is the barrier height at the grain boundary and is related directly to the carrier
 219 concentration according to

$$\Phi_B = \frac{e^2 n_t}{8\varepsilon_\infty \varepsilon_0 n_e} \quad (11)$$

220 where n_t is the trap density. The pre-factor μ_0 is the internal mobility of the grain, expressed
 221 as

$$\mu_0 = \frac{eL}{\sqrt{2\pi m_e k_B T}} \quad (12)$$

222 where L is the grain size. It is necessary to extend the Seto model in the case of degenerately
 223 doped ZnO to account for the tunnelling of carriers through the barrier Φ_B . As the carrier
 224 concentration increases the Fermi level rises towards the top of the barrier while the barrier
 225 height decreases proportionally to $1/n_e$. Following the onset of tunnelling the effective
 226 carrier mobility increases exponentially with respect to carrier concentration. The increase
 227 in mobility is eventually limited by other scattering processes, for example ionized-impurity
 228 scattering. A semi-empirical relationship the mobility due to the tunnelling of free carriers
 229 , μ_t can be expressed according to

$$\mu_t = \frac{\mu_{ii} - \mu_{ig}}{1 + \exp\left[-\frac{1}{\alpha}(\Delta_{BM} + E_R - \beta\Phi_B)\right]} \quad (13)$$

230 where the factor α accounts for the sharpness of the onset in tunnelling and is likely to
 231 be related to the depletion width of the grain boundary. A second empirical factor, β

approximates any extra functional dependence of Φ_B on n_t which is likely vary with respect to n_e . The effective mobility may therefore be expressed as the sum of the inter-grain and tunnel mobilities according to

$$\mu_{eff} = \mu_{ig} + \mu_t \quad (14)$$

Figure 7 shows the corresponding the fit of this extended model to the data. An extracted value of $n_t = 1.79 \times 10^{14} \text{ cm}^{-3}$ is over two orders of magnitude greater than that reported for reactively sputtered, undoped ZnO films [?] and an order of magnitude greater than that for Al doped ZnO films [?]. This is reflected in the relatively low optimum mobility values of $\sim 16 \text{ cm}^2\text{V}^{-1}\text{s}^{-1}$ which is typically half that of Al doped ZnO films. The reduction of the trap densities at the grain boundaries is therefore key to the improvement of carrier mobility in Si doped ZnO films. This is likely to be achieved through further investigations of the effect of growth parameters, i.e. substrate temperature and sputter pressure. Based on the model used in this work, a reduction of n_t by $\sim 20\%$ could yield a doubling of the mobility.

CONCLUSIONS

A consideration of the non-parabolicity of the conduction band for Si doped ZnO has yielded estimates for the values of the band minimum effective mass, $m_{e0} = 0.35m_0$, and the non-parabolicity factor, $C = 0.3 \text{ eV}^{-1}$. The non-parabolicity contributes to a reduction in the expected Burstein-Moss shift of the optical band-gap at carrier concentrations beyond 10^{20} cm^{-3} . Further reductions in the band-gap arises from the renormalization effects which are dominated by electron-electron and electron-ion interactions. For Si doped films the component of the magnitude of these effects are significantly greater than that reported for sputtered Al doped ZnO films.

The combinatorial methodology employed within this work allows the relationship between composition and the electrical behaviour to be determined with excellent accuracy, with a continuous distributions between n_e , μ_e , ρ and % wt. SiO_2 being determined. Furthermore, the extraction of all data from a single sample ensures that a high level of consistency between each data point is achieved compared with measurements taken over a series of separately deposited samples. Maximum values of $4.5 \times 10^{20} \text{ cm}^{-3}$ and $16 \text{ cm}^2\text{V}^{-1}\text{s}^{-1}$ were achieved for the carrier concentration and mobility respectively, at an optimal composition

261 of $x = 0.65\%$ wt. SiO_2 , and this corresponding to a minimum resistivity of $8.7 \times 10^{-4} \Omega\text{.cm}$.

262 The model of grain boundary scattering proposed by *Seto* [?] has been extended to
 263 include the effects of tunneling through grain boundaries. The model generates a good
 264 agreement for the observed μ_e versus n_e behaviour at compositions up to the optimum value
 265 of x . The model highlights a potential route to improving carrier mobility, i.e. by reducing
 266 the density of trap states that exist at the grain boundaries.

267 Above the optimum composition a different dependence is observed to that below it. This
 268 is thought to be due to the increased density of trap states associated with the incorporation
 269 of excess Si into the films.

270 The authors are grateful to Dr. Tim Veal for useful discussions concerning the work and
 271 to Vincent Vasey for technical assistance. This work was funded by EPSRC, grant number
 272 EP/F029624 and and EP/K018884/1.

273 * Corresponding Author: R.Treharne@liverpool.ac.uk

Parameter 1	Extracted Value	Copmparison [?]
$A (\times 10^{-8} \text{ eV.cm})$	2.1 ± 0.8	0.69
$B (\times 10^{-7} \text{ eV.cm}^{3/2})$	3.0 ± 2.6	1.6
$C (\times 10^{-7} \text{ eV.cm}^{3/4})$	8.7 ± 1.5	7.76
$E_{G0} (\text{eV})$	3.41 ± 0.01	-

TABLE I. Parameter values extracted from the downhill-simplex fit of equation 7 to the experimental data shown in figure 4. E_G values were extracted from fits to ellipsometry spectra taken in the vicinity of the band gap and n_e values were determined by Hall measurements. The coefficients A, B and C correspond to the amplitudes of the separate $n_e^{1/3}$, $n_e^{1/4}$, $n_e^{1/2}$ dependencies respectively of the renormalisation effects.

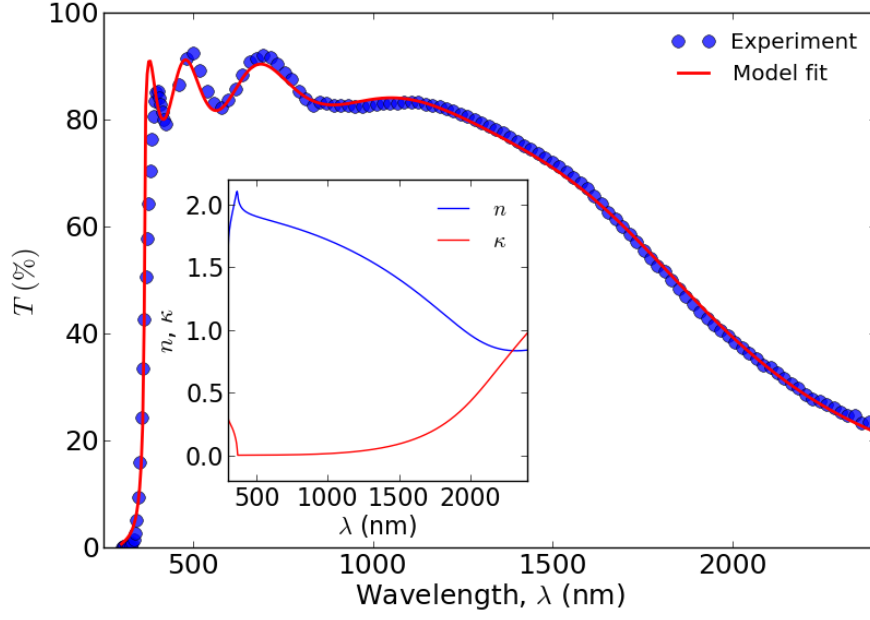


FIG. 1. Example of a typical transmittance curve taken from a single point on the combinatorial ZnO:Si sample. The line (—) shows the corresponding fit generated by the dielectric model [?]. An excellent fit is achieved at wavelengths in the vicinity of plasma edge, i.e. > 1000 nm. The band to band transition component of the model is insufficient to accurately describe the behaviour in the vicinity of the material's direct band gap. In this instance, values of $d = 518 \pm 10$ nm, $\varepsilon_{\infty}\omega_p = 0.97 \pm 0.02$ eV and $E_G = 3.38 \pm 0.04$ eV were extracted from the fitting procedure. The inset also shows the dispersion relationships for n and κ extracted by the model.

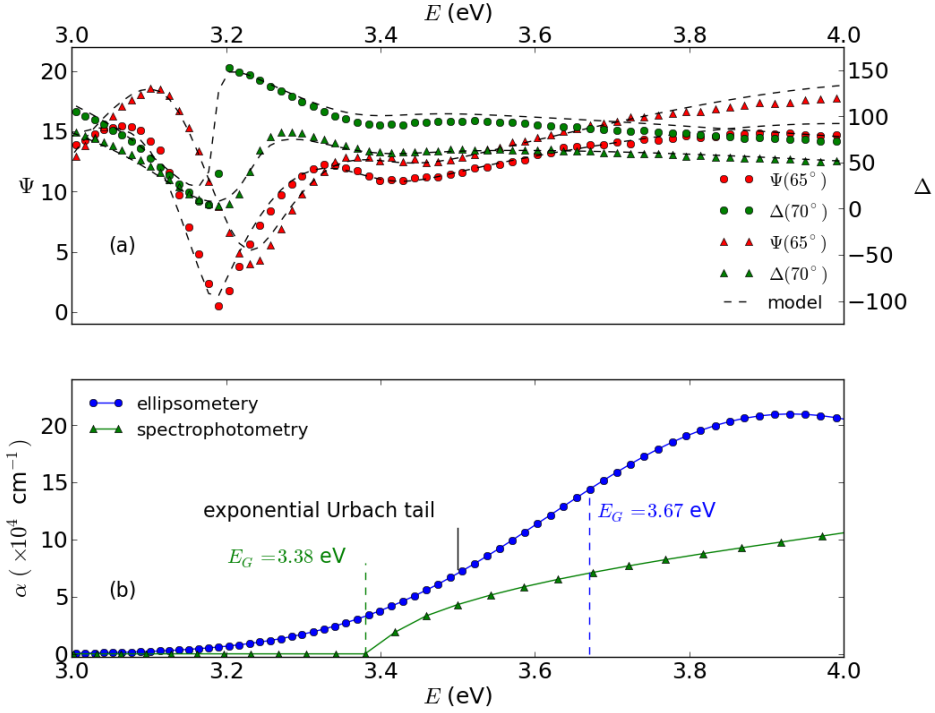


FIG. 2. a) Ellipsometric spectra (Ψ and Δ), measured at separate angles of 65° and 70° , were fitted over the range 3 eV (413 nm) to 4 eV (309 nm) using a single PSEMI-M0 oscillator [? ?], b) The corresponding absorption coefficient extracted from the ellipsometric data compared with that extracted from the spectrophotometric data (1). A difference in the direct band gap of ~ 0.3 eV is determined between the two optical extraction methods. The ellipsometric model is deemed to be more reliable due to its ability to account for the Urbach tail that arises from a distribution of impurity states located just below the bottom of the conduction band.

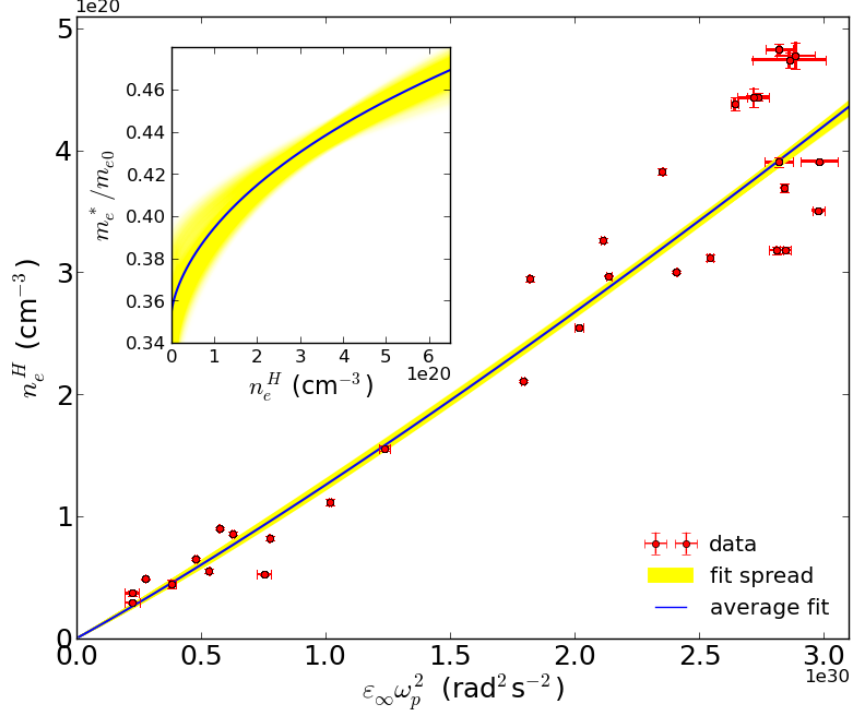


FIG. 3. Carrier concentration, n_e^H , determined via Hall effect measurements versus values of $(\epsilon_\infty \omega_p)^2$ extracted from the dielectric modeling of transmittance data. A Monte-Carlo style fitting procedure [?] indicates that the relationship between the axes is non-linear, as expected for a material with a non-parabolic conduction band. The spread in uncertainty associated with the fitting procedure is shown by the yellow line. The corresponding relationship between the carrier effective mass, m_e and the carrier concentration is shown in the inset. Values of $m_{e0} = 0.35 \pm 0.02 m_0$ and $C = 0.30 \pm 0.01 \text{ eV}^{-1}$ were extracted from the analysis.

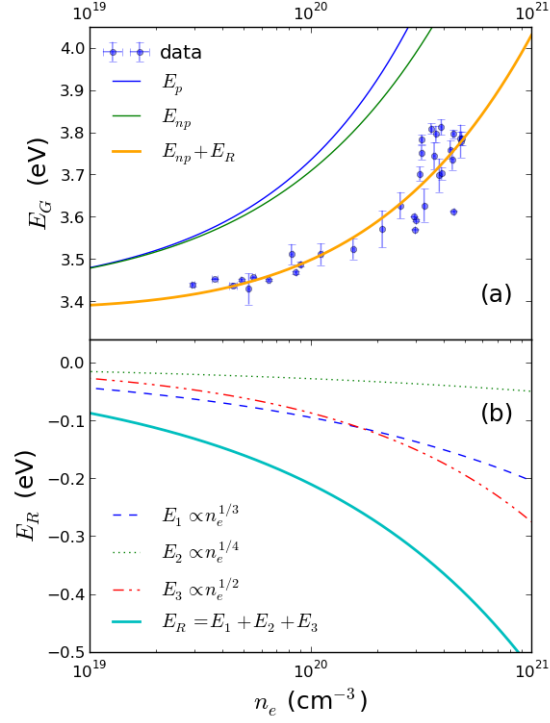


FIG. 4. a) Ellipsometry extracted band gap values, E_G , plotted with respect to the carrier concentration determined by Hall measurements. The Burstein-Moss relation (E_p), even once non-parabolicity is accounted for (E_{np}), is insufficient to predict the observed relationship - band gap values being significantly lower than expected. The incorporation of renormalization effects permits the data to be fitted. b) The total renormalization energy and each of its subcomponents are shown shown. The amplitude of these components is calculated empirically via a Monte-Carlo fitting procedure using the model proposed by [?].

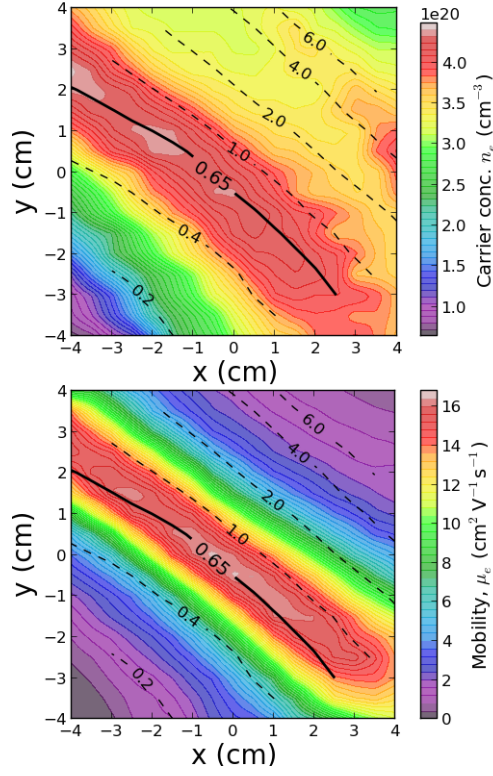


FIG. 5. 3D contour plots of the carrier concentration and mobility over the combinatorial sample. All values were extracted using the automated spectrophotometric mapping procedure. The (---) contour lines show an overlay of the % wt. SiO_2 composition.

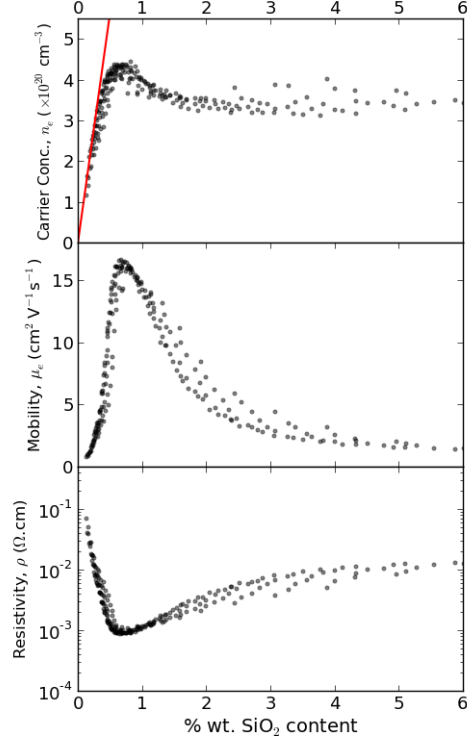


FIG. 6. Distributions of carrier concentration, mobility and resistivity with respect to % wt. SiO₂ content. The maximum values for n_e ($4.4 \times 10^{20} \text{ cm}^{-3}$) and μ_e ($16.5 \text{ cm}^2 \text{ V}^{-1} \text{ s}^{-1}$) coincide with a composition of 0.65% wt. SiO₂ and correspond to a minimum resistivity of 8.6 $\Omega \cdot \text{cm}$. The solid straight line (—) in the top plot shows the maximum theoretical carrier concentration achievable if every Si atom incorporated onto a zinc site contributes two free electrons to the system.

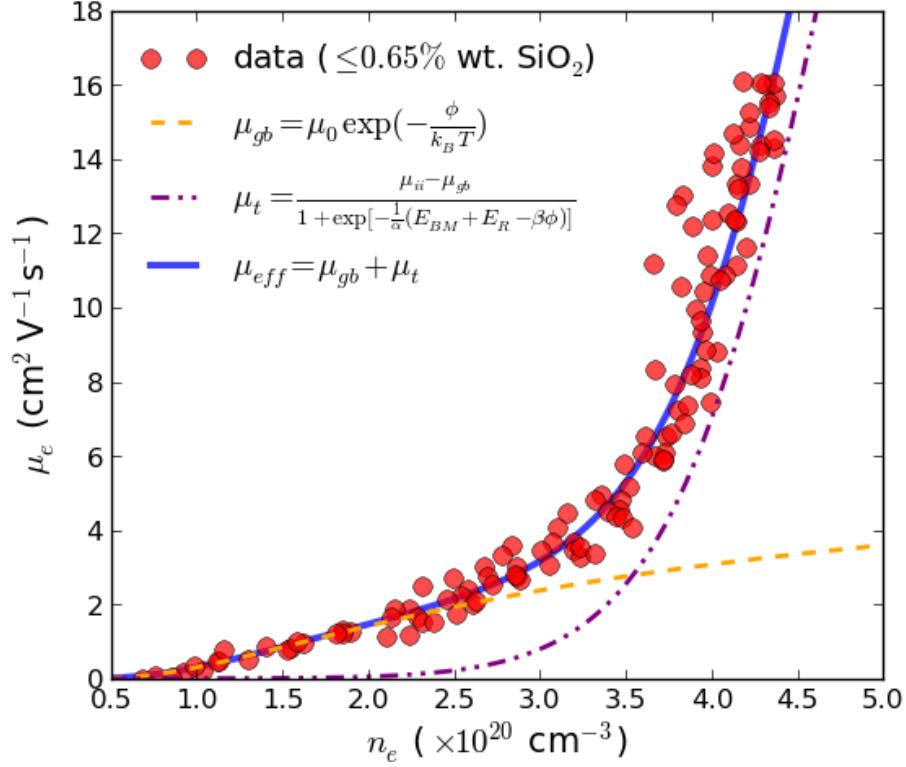


FIG. 7. Relationship between n_e and μ_e values extracted from the automated spectrophotometric mapping procedure. All data points have compositions below and up to the optimum value of 0.65% wt. SiO_2 . The line (—) shows the fit achieved to the data using equations 10-14. The parameter values $n_t = 1.7 \times 10^{14} \text{ cm}^{-2}$, $L = 40 \text{ nm}$, $\alpha = 25 \text{ eV}$ and $\beta = 0.54$ were extracted from a downhill-simplex fitting procedure [?]. An estimated value of $\mu_{ii} = 40 \text{ cm}^2\text{V}^{-1}\text{s}^{-1}$ was chosen for the fitting but the extracted values were shown to be relatively independent of μ_{ii} in the range $20 - 100 \text{ cm}^2\text{V}^{-1}\text{s}^{-1}$.